# Accepted Version

**To cite this version:**

A. Garcia-Tejero, M. Burgos-Garcia and F. Merli, "Broadband Metallized Plastic Waveguide Antenna With Robust Isolation Interface at 77 GHz," in IEEE Antennas and Wireless Propagation Letters, vol. 23, no. 10, pp. 2875-2879, Oct. 2024, doi: 10.1109/LAWP.2024.3412424

# Broadband Metalized Plastic Waveguide Antenna with Enhanced Low-Isolation Interface at 77 GHz

Alejandro Garcia-Tejero, Mateo Burgos-Garcia, Francesco Merli

***Abstract*—A two-layer metalized plastic waveguide antenna comprising a novel high-isolation interface for MIMO automotive radar at 76-81 GHz band is presented. The antenna contains three transmitters and four receivers. Each comprises an eight-horn linear array achieving a directivity of 16.0 dBi at 76.5 GHz. All individual antenna elements are connected to the PCB through an innovative compressed waveguide interface with polarization diversity and electromagnetic band gap (EBG) structures. The final prototype is fabricated employing injection molding, silver metallization, and soldering processes. Excellent overall performance is achieved, with a measured impedance bandwidth of 20.1%, and total efficiency up to 94% (-0.3 dB) for channels from 76-81 GHz. Furthermore, the interface offers minimal degradation over the antenna to PCB assembly tolerances (up to 400 um misalignment), maintaining coupling lower than -40 dB and realized gain difference within 0.3 dB. The design and its fabrication process are an attractive alternative to conventional substrate-based antennas.**

***Index Terms*—waveguide, horn antenna array, metalized plastic, injection molding, automotive radar, 76-81 GHz.**

## I. Introduction

Millimeter-wave radar sensors are one of the key elements in advanced driving assistance systems (ADAS). Antennas are one of its crucial parts as their performance significantly impacts the field-of-view (FOV), maximum range and angular estimation [1]. Thus far, primarily serial-fed microstrip [2], [3] or substrate integrated waveguide (SIW) antennas [4], [5] have been selected for automotive radar due to their low-profile and seamless integration with the other printed circuit board (PCB) components. Even though recent works from Lee et al. [6] improve impedance bandwidth and beamsquint, the substrate material limits the overall radiation efficiency, especially considering the routing from the antenna to the monolithic microwave integrated circuit (MMIC).

Alternative antennas based on propagation in air, such as an air-filled waveguide or gap waveguide (GW) [7], [8] overcome this limitation. Recently, Yue [9], and Ren [10] proposed 3-layer center-fed GW slot arrays manufactured by milling, both achieving high efficiency with low side-lobe levels (SLL) and impedance bandwidth between 3 to 9%. Tak et al. [11] presented an additive-manufactured slotted waveguide array antenna at W-band requiring multiple non-radiating slots on the waveguide to enable metallization, achieving a total efficiency of 65%. As these examples are manufactured using processes which can be challenging for mass production, a promising approach combining plastic injection molding with a metal coating has been introduced [12], [13] at E-band.

The integration of waveguide antennas poses challenges due to the interconnection with the MMIC, particularly in Multiple-Input-Multiple-Output (MIMO) systems with numerous channels. Microstrip-to-waveguide transitions [14], even including electromagnetic band gap structures (EBGs) [15], are common solutions. Seler [16] proposed the integration of numerous waveguide launchers within the MMIC package, placing the antenna directly on top of it. Ren [10] revealed results including EBGs achieving an isolation of -30 dB for moderate assembly tolerances (+/- 50 um). Moallem [17] proposed an alternative solution with an MMIC with integrated launchers at the bottom of the package. By this, the MMIC can be attached to one side of the PCB and directly feed a plated through waveguide section in the PCB that interconnects with the antenna on the other side. This work discloses a waveguide antenna system suitable for such an MMIC package. Furthermore, it includes novel features such as polarization diversity and EBGs to enhance isolation. Later, the interface is integrated into a highly efficient MIMO waveguide antenna and tested against real assembly tolerances.

## II. Interface and Antenna Design

This section discusses the proposed antenna design, from the PCB-waveguide interface to the single-element antenna and the complete architecture.

### A. Waveguide-PCB interface

A novel compressed waveguide interface based on a direct connection through a plated hole in the PCB [17] is implemented based on a 4x3 MMIC (four receivers and three transmitters) [18].

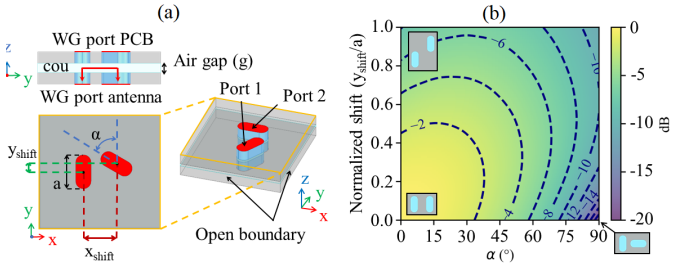


Fig. 1. (a) Schematic of the model (not in scale for z-axis): $g$ = 200 um. (b) Simulated normalized coupling (cou) in a waveguide-to-waveguide interconnect with different orientations ($x_{shift} = a$).

Alejandro Garcia-Tejero is with Microwave and Radar Group, Universidad Politecnica de Madrid, 28040 Madrid Spain, and with HUBER+SUHNER, 9000 Herisau, Switzerland. Mateo Burgos-Garcia is with Microwave and Radar Group, Universidad Politecnica de Madrid. Francesco Merli is with HUBER+SUHNER, 9000 Herisau, Switzerland. (e-mail: alejandro.garciatejero@hubersuhner.com)

In order to miniaturize the interface area, directly related to MMIC package size, placing broad wall waveguides in parallel must be avoided. Parallel narrow wall waveguides [10], minimize the area, although it maximizes coupling due to the shared polarization and position of electric field maximum. Varying the orientation among channels can provide extra isolation. Figure 1 reflects t he i nfluence in a waveguide-to-waveguide interconnect when shifting the channels in the Y-axis or rotating them, keeping its center-to-center distance ($x_{shift}$) constant. One can notice that the coupling decreases when increasing the shift further than $a/2$ or rotations with $\alpha > 45$. The most interesting results are obtained for neighbouring waveguides with $\alpha > 60$ and $y_{shift} < a/2$ with a coupling reduction up to 20 dB for a completely orthogonal waveguide without any shift. As a waveguide can only be surrounded by four direct neighbours (right, left, top and bottom) meeting this constraint, the rest of the openings must be diagonal to it. In that case, the optimal is to maintain at least $y_{shift}$ larger than $0.6a$ and preferably larger than $0.8a$.

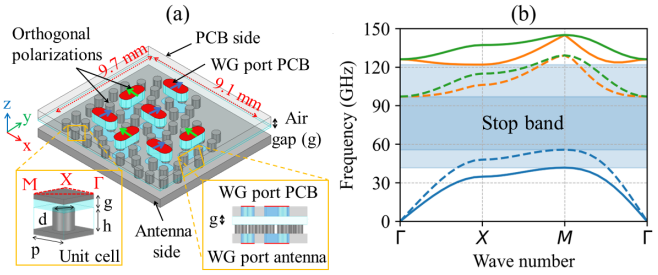


Fig. 2. (a) Dispersion diagram for $g$ = 100 um (solid) and $g$ = 400 um (dashed). (b) Unit cell and proposed waveguide-to-waveguide interface.

Figure 2(a) depicts the channel positions in the proposed interface. Each waveguide opening is orthogonal ($\alpha$ = 90°) and $y_{shift} < a/2$ to its neighbouring channels. Then, the diagonal waveguides are placed with $\alpha$ = 0° and $y_{shift} > 0.6a$, matching what is discussed above. Later, an E- or H-plane bend matches the port polarization with the waveguide routing.

Additionally, to compensate for undesired coupling due to assembly tolerances, a periodic structure can be introduced. It is of special interest the misalignment with the vertical axis, in the form of air gaps. A unit cell consisting of a metal plane facing a metallic pillar [19] with a height of 0.96 mm, a diameter of 0.85 mm, and a periodicity of 1.6 mm is designed. It achieves a simulated stop band between 41 to 122 GHz (99.3%) for an air gap ($g$) of 100 um between the pillar and the metal plane, as depicted in Figure 2(b). For $g$ = 400 um, the stop band reduces to 27.4% (from 56 GHz to 97 GHz), still fully covering the frequency of interest. Due to MMIC constraints in port positioning, the final EBG structure is pseudo-periodic, which may deteriorate slightly these values. In addition, the design incorporates an integrated double-ridge EBG waveguide opening [20] in the antenna side, which ensures the presence of a minimum of two pillars between adjacent channels with the same polarization, resulting in an increase in isolation levels larger than 10 dB compared to the single pillar case.

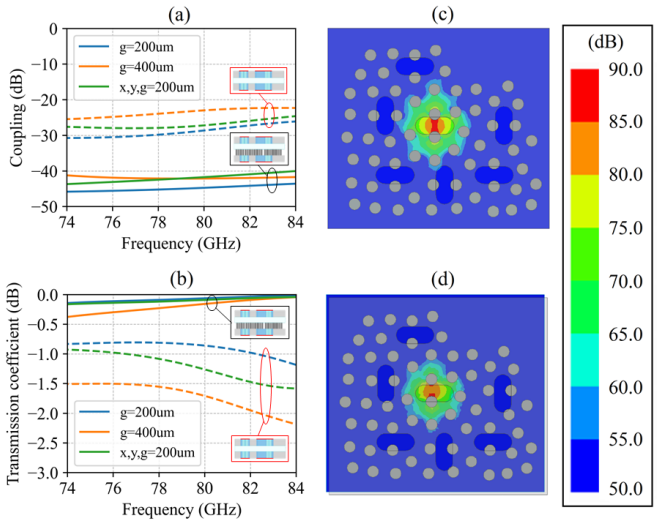


Fig. 3. Worst case interface coupling (a) and transmission coefficient (b) for different air gaps ($g$) and planar $(x, y)$ misalignment between antenna and waveguide fed. (solid) Pseudo-periodic EBG interconnect, (dashed) non-EBG interconnect. 2D Electric field when transmitting from the center port (c) $g = 400um$ and (d) $(x, y, z) = 200um$.

Figure 3 compares simulations of the highest port-to-port coupling (a) and the lowest transmission coefficient (b) for a plated hole to waveguide interconnect with polarization diversity (dashed) and one including the pseudo-periodically structure (solid) for different cases of tolerance of air gap ($g$) and planar $(x, y)$ misalignment. The interface without EBG structure achieves a coupling between -30 to -22 dB and a transmission coefficient worse than -1.7 dB. The proposed solution obtains a coupling between -45 to -40 dB, and a transmission coefficient higher than -0.5 dB even for an air gap ($g$) of 400 um. Finally, in Figure 3(c) and (d) the electric field for the cases of tolerance is depicted. It can be appreciated how the field is concentrated within one row of pillars.

### *B. Single-element antenna and waveguide routing*

The antenna is conceived as a split-block waveguide of only two layers. The design consists of a linear waveguide horn array with eight elements to reach a narrow elevation pattern and broad azimuth, enabling beamforming and achieving a realized gain of roughly 15.7 dBi at 76.5 GHz. A broad impedance matching covering the 76-81 GHz band at -15 dB is obtained. Further details on the design can be found on [13].

An internal waveguide routing is required to connect the individual antennas to the MMIC. An appropriate waveguide partition is needed to minimize losses. The waveguide is split in its E-field maximum, where the currents are null [21], see Figure 4(d). Routing has been equalized in phase to simplify radar calibration further. Therefore all routings maintain the same electrical length or multiples of $\lambda_g/2$. The average routing length is 25 mm, with the shortest being 12 mm and the longest 42 mm, with a difference of five $\lambda_g$.

### *C. Single-element antenna placement*

The placement of single elements was determined through a trade-off aimed at minimizing over-the-air cross-talk while

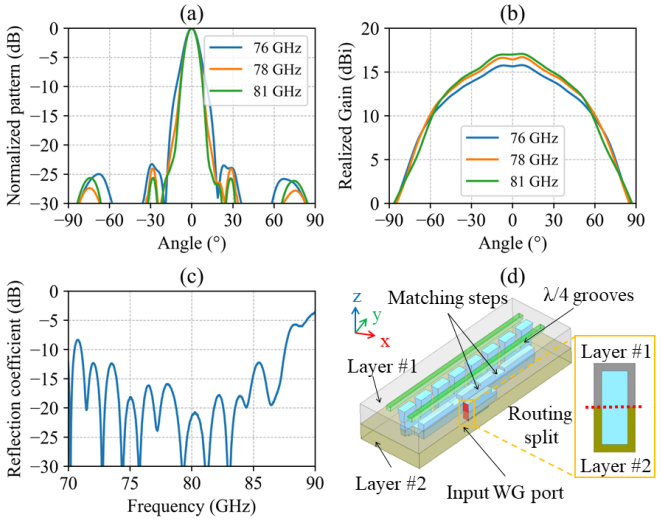


Fig. 4. Simulated single-element performance: (a) elevation normalized pattern, (b) azimuth realized gain pattern. (c) reflection coefficient. Sketch of the two-layer single-element antenna design and split of routing in (d). Grey and copper color scales represent metal, blue vacuum.

maximizing the population of $\lambda_0/2$ elements within the virtual array, as demonstrated in Figure 5(a).

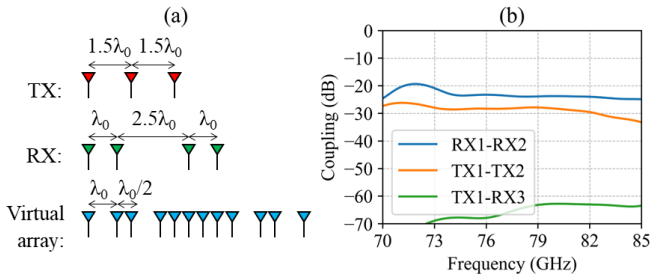


Fig. 5. (a) Position of single-element antennas. (b) Simulated radiation coupling of the worst antenna-to-antenna combinations (considering lossless metal and no internal routing).

Given the very low loss of air-filled waveguide antennas, isolation is mainly driven by the coupling of the PCB-waveguide interface (Figure 3) and the coupling among different single elements. The latest one can be tackled by the introduction of grooves between the channels [22], achieving a worst radiated coupling of -25 dB for RX-RX, -30 dB for TX-TX and lower than -60 dB for RX-TX (Figure 5(b)).

## III. Manufacturing

A plastic injection molding process is used to manufacture both layers of the split-block, resulting in precise shapes that are highly repeatable and cost-effective for large-scale production. After that, the plastic parts are silver coated. Ultimately, the layers are joined by a high-temperature soldering process to ensure optimal total efficiency without any leakage or any other source of crosstalk. All described operations were performed at HUBER+SUHNER premises [23] in Switzerland. The front and back side of the manufactured prototype is shown in Figure 6.

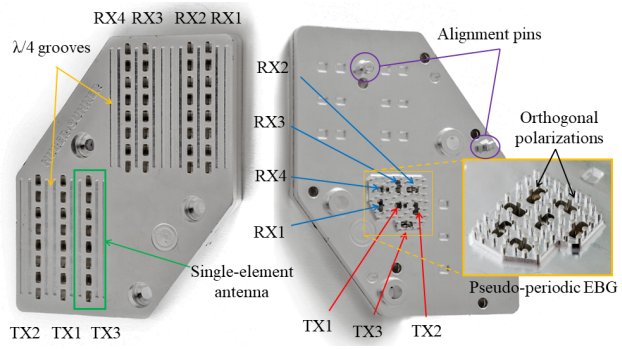


Fig. 6. Manufactured prototype. Front side (left) and back side highlighting EBG-based interface (right).

## IV. Experimental Results and Tolerance

The setup depicted in Figure 7 was used to measure the S-parameters. An adaptor jig matches the antenna opening to a standard WR-12. In order to verify the performance with potential air gaps when assembling the waveguide to the PCB, different spacers (from 0 to 400 um) can be placed between the antenna and the adaptor (tolerance cases).

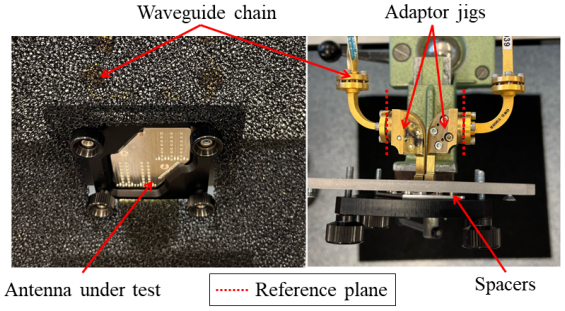


Fig. 7. Setup for S-parameters measurement.

The prototype reflection coefficient for all antenna channels and tolerances cases (i.e. spacers) is shown in Figure 8. It is worth mentioning that the nominal prototype demonstrates excellent impedance matching, with a reflection coefficient below -14 dB in the 76-81 GHz band and below -10 dB between 73 to 82.1 GHz for all the single channels. When analyzing tolerance scenarios, it can be observed how adding spacers increases the reflection. Acceptable performance is exhibited up to 300 um air gap, and finally, with 400 um, two channels are above -10 dB.

The highest cases of TX-TX, RX-RX, and RX-TX coupling for nominal and tolerances cases are presented in Figure 9. Despite adding spacers, the isolation remains stable without significant variations for the TX-TX and RX-RX levels since the radiation cross-talk dominates, and the coupling at the interface is still low in comparison. For RX-TX, the radiation coupling between antenna elements is almost negligible (lower than -60 dB in simulations). Hence, it is observed that the coupling level increases gradually with each spacer addition, with a maximum level of -45 dB for the 400 um case. All these levels agree with the tolerance simulations.

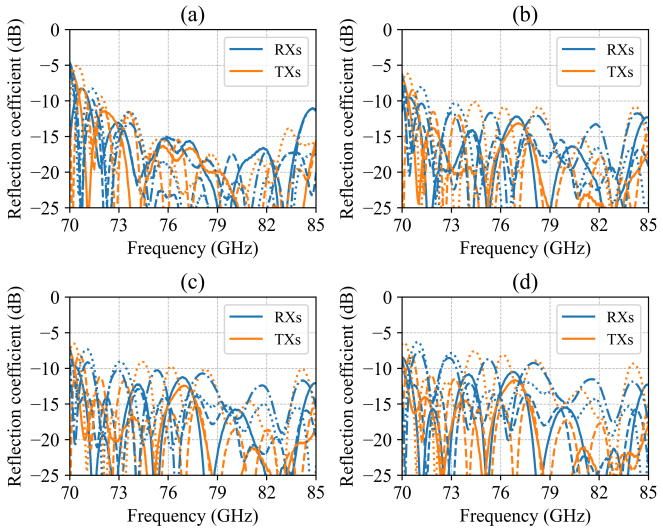


Fig. 8. Reflection coefficient measurement results for RX and TX. (a) Nominal. (b) 200 um air gap. (c) 300 um air gap. (d) 400 um air gap.

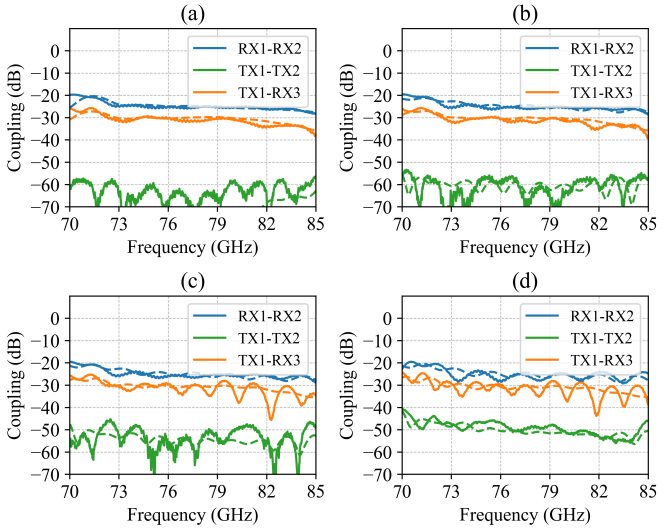


Fig. 9. Coupling measurement results (solid) and simulated (dashed). (a) Nominal (b) 200 um air gap. (c) 300 um air gap. (d) 400 um air gap.

Figure 10(a) and (b) depict the pattern measurement and simulations for RX1 and TX1 at 76, 78, and 81 GHz. The results show a perfect agreement with simulations indicating that an elevation half power beamwidth (HPBW) lower than 9° in the band of interest. Figure 10(c) and (d) show the measured and simulated performance over those channels. The measured realized gain is higher than 15.4 dBi, and the SLL is lower than -18, and -22 dB respectively. TX1 presents a lower gain due to its lower directivity as can be seen in the azimuth pattern in the previous figure. The total efficiency is up to 94%.

Additionally, two tolerance measurements were performed: nominal and 400 um air gap tolerance for the TX1 antenna, which corresponds to the worst coupling case since this channel is completely surrounded by all the others. Figure 11 shows pattern simulations and measurements at 76 and 81 GHz, realized gain and efficiency over the whole band. Negligible

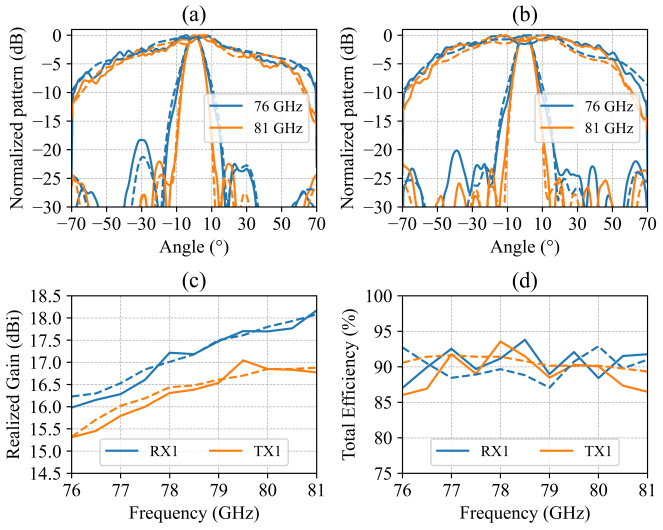


Fig. 10. Simulation (dashed) and measurements (solid) of azimuth and elevation normalized pattern of RX1(a) and TX1(b). Simulation (dashed) and measurements (solid) of realized gain (c) and efficiency (d) over frequency.

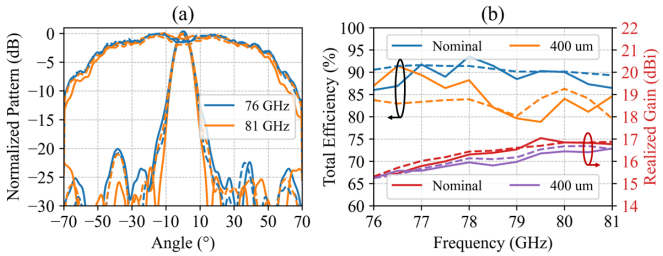


Fig. 11. (a) TX1 Azimuth and Elevation pattern measurements at 76 GHz and 81 GHz: (solid) Nominal, (dashed) 400 um air gap. (b) TX1 Total efficiency and realized gain: measurements (solid) and simulations (dashed).

differences between the nominal and tolerance cases can be observed. Pattern shape is essentially preserved; minor differences in secondary side-lobe levels, and the gain difference are lower than 0.5 dB, consistent with the difference in reflection coefficient and proportionally to mismatch loss.

## V. Conclusion

A waveguide antenna for MIMO mid-range automotive radar at 77 GHz was developed. The antenna consists of seven single-element channels comprising an eight-horn linear array. The single-element design reaches 16.0 dBi of directivity. A robust compressed PCB-waveguide interface with polarization diversity and EBG structures was designed.

The manufactured prototype employed two pieces of metallized plastic using injection molding, PVD, electroplating, and soldering processes. Outstanding free-space performance was achieved with a total efficiency of up to 94% and an extensive impedance bandwidth of up to 16.5 GHz. Measurement studies on assembly tolerances were performed, achieving negligible degradation for realized gain and channel coupling under extreme tolerance cases. Thus, the built prototype is a proof of concept for high efficiency, large bandwidth, and low-cost antenna solutions suitable for mm-wave sensors.

## REFERENCES

[1] J. Hasch, E. Topak, R. Schnabel, T. Zwick, R. Weigel, and C. Waldschmidt, "Millimeter-wave technology for automotive radar sensors in the 77 ghz frequency band," *IEEE Transactions on Microwave Theory and Techniques*, vol. 60, no. 3, pp. 845–860, 2012.

[2] W. Menzel and A. Moebius, "Antenna concepts for millimeter-wave automotive radar sensors," *Proceedings of the IEEE*, vol. 100, no. 7, pp. 2372–2379, 2012.

[3] X. Wang and A. Stelzer, "A 79-ghz ltcc patch array antenna using a laminated waveguide-based vertical parallel feed," *IEEE Antennas and Wireless Propagation Letters*, vol. 12, pp. 987–990, 2013.

[4] S. Cheng, H. Yousef, and H. Kratz, "79 ghz slot antennas based on substrate integrated waveguides (siw) in a flexible printed circuit board," *IEEE Transactions on Antennas and Propagation*, vol. 57, no. 1, pp. 64–71, 2009.

[5] F. Bauer and W. Menzel, "A 79-ghz planar antenna array using ceramic-filled cavity resonators in ltcc," *IEEE Antennas and Wireless Propagation Letters*, vol. 12, pp. 910–913, 2013.

[6] J.-H. Lee, J. M. Lee, K. C. Hwang, D.-W. Seo, D. Shin, and C. Lee, "Capacitively coupled microstrip comb-line array antennas for millimeter-wave applications," *IEEE Antennas and Wireless Propagation Letters*, vol. 19, no. 8, pp. 1336–1339, 2020.

[7] F. J. Sanchez Vazquez and R. Pearson, "Waveguide," *European Patent*, no. 1331688, Jan. 29 2002.

[8] P.-S. Kildal, E. Alfonso, A. Valero-Nogueira, and E. Rajo-Iglesias, "Local metamaterial-based waveguides in gaps between parallel metal plates," *IEEE Antennas and Wireless Propagation Letters*, vol. 8, pp. 84–87, 2009.

[9] J. Yue, C. Zhou, K. Xiao, L. Ding, and S. Chai, "W-band low-sidelobe series-fed slot array antenna based on groove gap waveguide," *IEEE Antennas and Wireless Propagation Letters*, vol. 22, no. 4, pp. 908–912, 2023.

[10] Q. Ren, C. Bencivenni, G. Carluccio, H. T. Shivamurthy, A. De Graauw, F. Jansen, J. Yang, and A. U. Zaman, "Gapwaveguide automotive imaging radar antenna with launcher in package technology," *IEEE Access*, vol. 11, pp. 37 483–37 493, 2023.

[11] J. Tak, A. Kantemur, Y. Sharma, and H. Xin, "A 3-d-printed w-band slotted waveguide array antenna optimized using machine learning," *IEEE Antennas and Wireless Propagation Letters*, vol. 17, no. 11, pp. 2008–2012, 2018.

[12] Y. Hirayama, K. Sakakibara, H. Umemura, K. Miyazaki, and N. Kikuma, "Effect of wall-surrounded slot on stepped narrow wall for bandwidth enhancement of partially parallel-feeding waveguide traveling-wave array," *IEEE Transactions on Antennas and Propagation*, vol. 65, no. 8, pp. 3976–3985, 2017.

[13] A. Garcia-Tejero, M. Burgos-Garcia, and F. Merli, "High-efficiency injection-molded waveguide horn antenna array for 76-81 ghz automotive radar applications," in *2022 19th European Radar Conference (EuRAD)*, 2022, pp. 21–24.

[14] Z. Tong and A. Stelzer, "A vertical transition between rectangular waveguide and coupled microstrip lines," *IEEE Microwave and Wireless Components Letters*, vol. 22, no. 5, pp. 251–253, 2012.

[15] A. A. Brazález, E. Rajo-Iglesias, J. L. Vázquez-Roy, A. Vosoogh, and P.-S. Kildal, "Design and validation of microstrip gap waveguides and their transitions to rectangular waveguide, for millimeter-wave applications," *IEEE Transactions on Microwave Theory and Techniques*, vol. 63, no. 12, pp. 4035–4050, 2015.

[16] E. Seler, M. Wojnowski, W. Hartner, W. Sörgel, J. Böck, R. Lachner, J. Hasch, and R. Weigel, "Chip-to-rectangular waveguide transition realized in embedded wafer level ball grid array (ewlb) package," in *WAMICON 2014*, 2014, pp. 1–4.

[17] M. Moallem and B. Ginsburg, "Grounded bga wave-guiding interface," *European Patent*, no. 3970237, May. 14 2019.

[18] B. P. Ginsburg, K. Subburaj, S. Samala, K. Ramasubramanian, J. Singh, S. Bhatara, S. Murali, D. Breen, M. Moallem, K. Dandu, S. Jalan, N. Nayak, R. Sachdev, I. Prathapan, K. Bhatia, T. Davis, E. Seok, H. Parthasarathy, R. Chatterjee, V. Srinivasan, V. Giannini, A. Kumar, R. Kulak, S. Ram, P. Gupta, Z. Parkar, S. Bhardwaj, Y. C. Rakesh, K. A. Rajagopal, A. Shrimali, and V. Rentala, "A multimode 76-to-81ghz automotive radar transceiver with autonomous monitoring," in *2018 IEEE International Solid - State Circuits Conference - (ISSCC)*, 2018, pp. 158–160.

[19] E. Rajo-Iglesias, A. U. Zaman, and P.-S. Kildal, "Parallel plate cavity mode suppression in microstrip circuit packages using a lid of nails," *IEEE Microwave and Wireless Components Letters*, vol. 20, no. 1, pp. 31–33, 2010.

[20] R. Glogowski and U. Huegel, "Adapter structure with waveguide channels," *European Patent*, no. 3479437, Jun. 29, 2016.

[21] J. Hesler, "A photonic crystal joint (pcj) for metal waveguides," in *2001 IEEE MTT-S International Microwave Sympsoium Digest (Cat. No.01CH37157)*, vol. 2, 2001, pp. 783–786 vol.2.

[22] R. Glogowski and U. Huegel, "Array antenna," *European Patent*, no. 17735041, Mar. 3, 2016.

[23] U. Huegel, A. Garcia-Tejero, R. Glogowski, E. Willmann, M. Pieper, and F. Merli, "3d waveguide metallized plastic antennas aim to revolutionize automotive radar." *Microwave Journal*, vol. 65, no. 9, 2022.